Exact Solutions to Collisionless External Gas Flow Problems

Chunpei Cai[a, *] and Quanhua Sun[b]

[a]*Department of Mechanical & Aerospace Engineering, New Mexico State University*
*Las Cruces, New Mexico State, 88003-8001, USA (*Email: *ccai@nmsu.edu)*
[b]*LHD, Institute of Mechanics, Chinese Academy of Sciences, Beijing, 100190, China*

Abstract. This paper presents exact density, velocity and temperature solutions for two problems of collisionless gas flows around a flat plate or a spherical object. At any point off the object, the local velocity distribution function consists of two pieces of Maxwellian distributions: one for the free stream which is characterized by free stream density, temperature and average velocity, n_0, T_0, U_0; and the other is for the wall and it is characterized by density at wall and wall temperature, n_w,T_w. Directly integrating the distribution functions leads to complex but exact flowfield solutions. To validate these solutions, we perform numerical simulations with the direct simulation Monte Carlo (DSMC) method. In general, the analytical and numerical results are virtually identical. The evaluation of these analytical solutions only requires less than one minute while the DSMC simulations require several days.

Keywords: Collisionless Flows, Free Molecular Flows, direct simulation Monte Carlo
PACS: 47.45Dt/47.61Fg/44.10+i/42.27ek

INTRODUCTION

Collisionless gas flow field over a flat plate or a sphere have many applications. The corresponding aerodynamic coefficients and heat flux rate are important for spacecraft design. Some flow examples include highly rarefied gas flows around: 1) a flat cryogenic vacuum pump; 2) a very small pollen or a pollutant particle; 3) a lunar dust particle in a moon-landing mission; 4) an aerosol droplet at high altitude; 5) a fine metal powder particle during a thin film deposition processing inside a vacuum chamber; 6) a meteoroid traveling in space; 7) a small cold sphere with condensation effect; 8) a spacecraft in low earth orbit with out-gassing.

For such flows, the earliest work may date back to Epstein [1] or Liu [2]; several recent books discussed collisionless aerodynamics over a flat plate or a sphere as well. Especially, Bird [3] discussed plate surface properties for collisionless flows with both diffuse and specular reflections, and the direct simulation Monte Carlo (DSMC) method is one appropriate numerical tool to simulate such kind of gas flows. Recently, Loth [4] reviewed compressibility and rarefication effects on drag over a small sphere. Storch [5] provided more detailed discussion on the aerodynamic coefficient for different objects. In the literature, almost all work on collisionless flows over a flat plate or a sphere focuses on the wall properties. It seems that the flowfield around a plate or a sphere should be very simple without any collision effects, but available research work in the literature concentrates on numerical simulations only. This paper aims to provide the exact solutions for the collisionless gas flow over a plate or a sphere, and these solutions complement the past studies on aerodynamic coefficients and heat transfer rate.

In this study, we use a relation between velocity-directions and geometry-locations to investigate free molecular flow problems.[6] This treatment is more general than the solid angle treatment by Narasimha [7], which is widely used for true collisionless effusion flows with a zero average speed, but it is not applicable to collisionless flows with a nonzero average speed. The object surfaces are assumed to be completely diffuse.

COLLISIONLESS GAS FLOWS OVER A FLAT PLATE

A zero-thickness flat plate AB is set with an inclination angle, ξ, to the free stream, with a length L. The coordinate center is at the plate center. Steady free stream collisionless gas flows from the left to the right, with a

number density, n_0, an average velocity, U_0 and a temperature, T_0. We are about to find the flow field around the plate.

We assume the outer boundary as a circle with a large radius. At each point on the circle, particles traveling from far field follow a Maxwellian velocity distribution function (VDF) characterized by n_0, U_0 and T_0. Suppose there is an arbitrary point P(x, y) off the plate (either in the front or the back side of the plate) and this section aims to obtain the exact flow field at P(x,y). The distribution for those reflected molecules is also a Maxwellian VDF characterized by the wall temperature, T_w, and a number density characterized by wall, n_w. We completely ignore interactions among molecules.

Starting from a point (X,Y) on the large circle, of all particles with a thermal velocity (u,v,w) only those satisfying the following relation can reach point P(x,y) if (X,Y) is "visible" from point P:

$$(u+U_0)/(X-x) = v/(Y-y) \tag{1}$$

Here $u+U_0$ is the real X-velocity speed for the particles traveling from the free stream. If on (X,Y) a particle's velocity components satisfy the above relation, then this particle cannot miss P(x,y) either, unless it is on the other side of the plate. Because all particles traveling towards the plate on the large circle follow the free stream Maxwellian VDF, this relation leads to a specific velocity space as Ω_1. With a similar relation,

$$u/(X-x)=v/(Y-y) \tag{2}$$

the contribution to the VDF at P(x,y) by those particles diffusely reflected on the plate is described by another Maxwellian VDF with a domain Ω_2. Here these particles have different velocities from those traveling from the free stream. The boundaries of these two domains, Ω_1 and Ω_2, are determined by point P(x,y), the two specific plate ends, A(Ax,Ay), B(Bx,By), and the above Eqns.(1-2). If we denote θ_1=arctan(y-Ay, x-Ax) and θ_2=arctan(y-By, x-Bx) here arctan(y,x) is a special function with a value range of $(-\pi, \pi)$, instead of $(-\pi/2, \pi/2)$. From Eqn.(1), we conclude that point (-U,0) belongs to domain Ω_1. In general, Ω_1 overlaps with Ω_2; one exception is the case with U_0=0 and a combination of Ω_1 and Ω_2 leads to a complete four-quadrant domain.

The VDF for point P(x,y) consists of two different Maxwellian VDFs:

$$f_0(u,v,w) = n_0(\beta_0/\pi)^{3/2}\exp[-\beta_0(u^2+v^2+w^2)], u/v \in \Omega_1, \tag{3}$$

$$f_w(u,v,w) = n_w(\beta_w/\pi)^{3/2}\exp[-\beta_w(u^2+v^2+w^2)], u/v \in \Omega_2, \tag{4}$$

where $\beta_i=1/(2RT_i)$, i=0, w, and n_w is:

$$n_w = n_0\sqrt{T_0/T_w}[\exp(-S^2S_\eta^2)+\sqrt{\pi}(SS_\eta)[1+\mathrm{erf}(SS_\eta)]]. \tag{5}$$

where $S = U_0\beta_0^{1/2}$ is the speed ratio, and S_η = -cos η with η the angle between the flow direction and the local surface normal. Integrating Eqns.(3,4) with different moments provides the density, velocity and temperature:

$$n(x,y)/n_0 = 1-\frac{1}{2\pi}\exp(-\beta_0U_0^2)[(\theta_2-\theta_1)+\sqrt{\pi}\gamma_1(\theta_1,\theta_2)]+\frac{n_w}{2\pi n_0}(\theta_2-\theta_1), \tag{6}$$

where $\gamma_1(\theta_1,\theta_2) = \int_{\theta_1}^{\theta_2}\exp(\beta_0U_0^2\cos^2\theta)\sqrt{\beta_0}U_0\cos\theta[1+\mathrm{erf}(\sqrt{\beta_0}U_0\cos\theta)]d\theta$

$$\sqrt{\beta_0}U(x,y) = -\frac{n_0\sqrt{\beta_0}\exp(-\beta_0U_0^2)}{2n\pi}(\sqrt{\beta_0\pi}\gamma_2(\theta_1,\theta_2)+\gamma_1(\theta_1,\theta_2)\frac{\sqrt{\pi}}{2\beta_0U_0}+\frac{U_0(\theta_2-\theta_1)}{2}+ \frac{U_0[\sin(2\theta_2)-\sin(2\theta_1)]}{4})+\frac{n_0U_0\sqrt{\beta_0}}{n}+\frac{n_w(\sin\theta_2-\sin\theta_1)}{4\sqrt{\pi}n}\sqrt{\frac{T_w}{T_0}}, \tag{7}$$

where $\gamma_2(\theta_1,\theta_2) = \int_{\theta_1}^{\theta_2}(U_0^2\cos^3\theta[1+\mathrm{erf}(\sqrt{\beta_0}U_0\cos\theta)]\exp(\beta_0U_0^2\cos^2\theta))d\theta$. With a= -$U_0$cosθ, we have:

$$\frac{T(x,y)}{T_0} = T_wn_w\frac{\theta_2-\theta_1}{2\pi nT_0}+\frac{n_0}{n}(1+\frac{U_0^2}{3RT_0})-\frac{n_0\exp(-\beta_0U_0^2)}{6\pi n}((3+\frac{U_0^2}{2RT_0})(\theta_2-\theta_1)+\frac{U_0^2[\sin(2\theta_2)-\sin(2\theta_1)]}{4RT_0})+ \frac{n_0}{6nRT_0}\sqrt{\frac{\beta_0}{\pi}}[\int_{\theta_1}^{\theta_2}\exp(-\beta_0U_0^2\sin^2\theta)(a^3+2a/\beta_0)[1+\mathrm{erf}(U_0\cos\theta\sqrt{\beta_0})]d\theta]-\frac{U^2+V^2}{3RT_0}. \tag{8}$$

To validate the above results, we performed a simulation with the direct simulation Monte Carlo (DSMC) method, and we turned off the collision function inside the simulation package. Figures 1 and 2 show density, temperature and velocity contours for a plate with a plate inclination angle of 30°. The plate surface facing the free stream flow has higher density and lower U-velocity due to the blockage effect, and the lee side has lower number density with some locations having higher U-velocity. This case provides complex patterns, the analytical and numerical results are almost identical except around the two plate tips. Cai [8] recently reported how to determine cryogenic pump plate sticking coefficient with measured local properties.

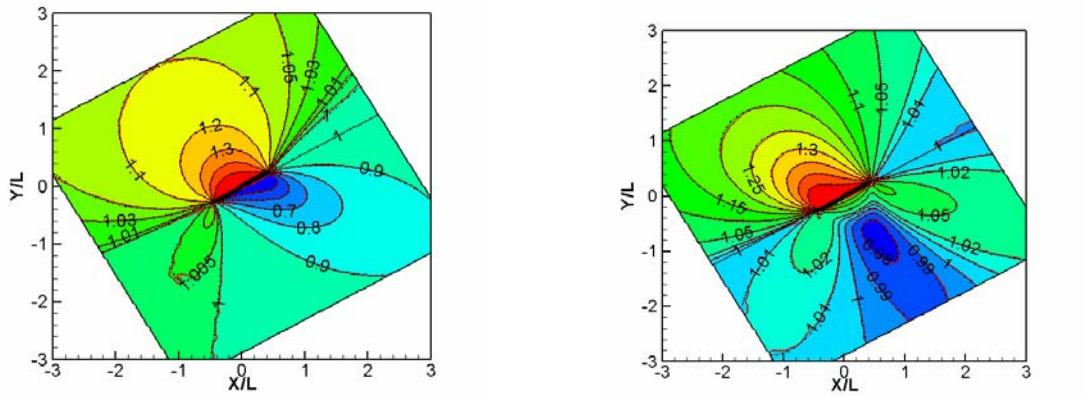

FIGURE 1. Contours of normalized density (left) and temperature (right), for collisionless gas flows around a flat plate, 30^o inclination angle, S=1, T_w =300 K, T_0=200 K. Dashed line: analytical, solid line: DSMC.

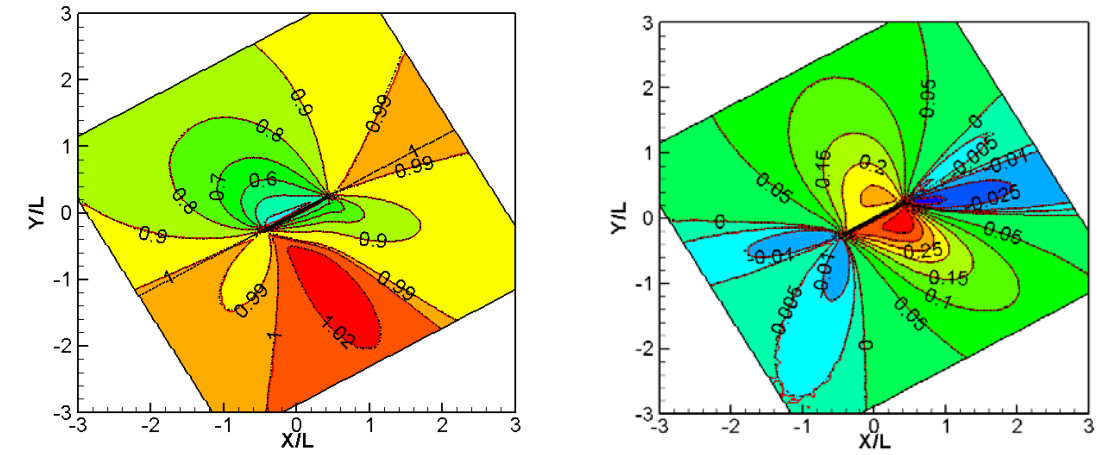

FIGURE 2. Contours of U-velocity (left) and V-velocity (right), for collisionless gas flows around a flat plate, 30^o inclination angle, S=1, T_w =300 K, T_0=200 K. Dashed line: analytical, solid line: DSMC.

COLLISIONLESS GAS FLOW OVER A SPHERICAL OBJECT

As shown by the left one in Figure 3, suppose inside the X-Z plane, there is a point P(X,0,Z) off the sphere, with a given collisionless free stream flowing along the X-axis direction, and the parameters are n_0, U_0, and T_0, we are about to compute the flow field at point P. If we suppose $\angle POX = \alpha$, then probably a more convenient way to compute the flow field is to rotate the axis counterclockwise with a value of π/2-α. After the computation of the local property at $P'(0,0,\sqrt{X^2+Z^2})$, we rotate back to the original coordinate system. In the rotated system, for point P', the local velocity distribution function consists of two parts:

$$f_0(u,v,w) = n_0(\beta_0/\pi)^{3/2} \exp[-\beta_0(u^2+v^2+w^2)], (u,v,w) \in \Omega_1, \quad (9)$$

$$f_w(u,v,w) = n_w(\beta_w/\pi)^{3/2} \exp[-\beta_w(u^2+v^2+w^2)], (u,v,w) \in \Omega_2, \quad (10)$$

where Ω_1 and Ω_2 represent the velocity space for free stream and the wall shadow regions respectively; n_w in the above equation is not constant, and its computation is illustrated with Fig. 3 (right). Ω_2 can be illustrated by the top conical region above point P', there is one point q with coordinates r=R', θ=θ', and ε=ε' in the spherical coordinate (r, θ, ε) where $0<\theta<\theta_0$ and $0<\varepsilon<2\pi$, then the function n_w there can trace backwards through a ray passing point P', and intersect the bottom sphere at point q'. With simple geometry relations we can obtain the coordinates for point $q'(oq', \theta, \varepsilon+\pi)$: $\angle q'p'O = \theta$, $\sin(\angle P'q'O)/\sqrt{X^2+Z^2} = \sin(\theta)/R_0$, and $\angle p'Oq' = \pi - \theta - \angle q'p'O$. Based on these fixed

coordinates, we can compute the normal components (n_x, n_y, n_z) on the sphere for point p'. In the new coordinate system, the flow direction is (cos(π/2-α), 0, sin(π/2-α)), and we can compute the angle ζ between the free stream and the sphere normal at q': $\cos\zeta = n_x\sin\alpha + n_z\cos\alpha$. Then the density at wall is, if $S_\zeta = -\cos\zeta$:

$$n_w = n_0\sqrt{T_0/T_w}[\exp(-S^2S_\zeta^2) + \sqrt{\pi}(SS_\zeta)[1+erf(SS_\zeta)]], \tag{11}$$

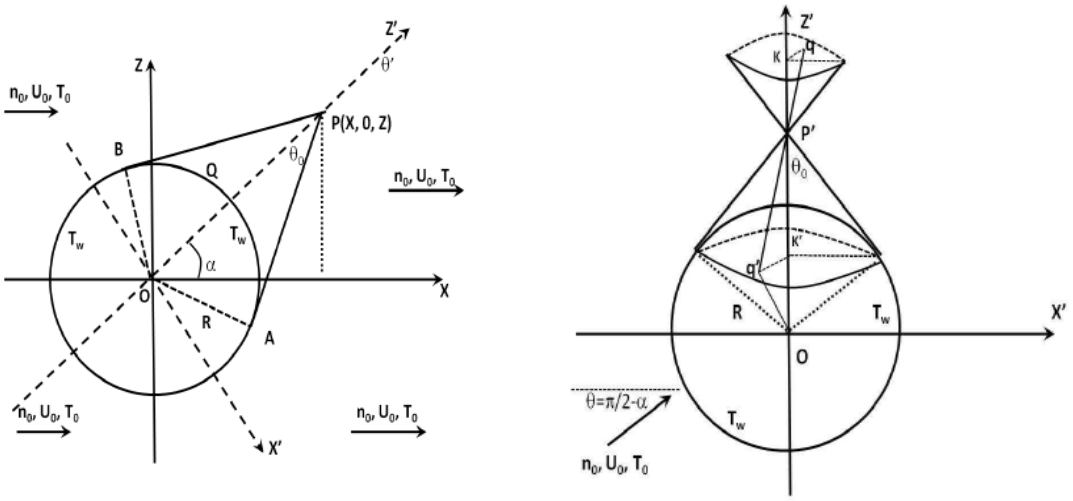

FIGURE 3. Illustration of the sphere problem:orginal position(left); rotated postion & part of velocity space(right).

Integrating the above two velocity distribution functions, Eqns. (9) and (10), over 1, u, v, (u2+v2+w2)/2, leads to the macroscopic number density, velocity components and temperature distributions for the new coordinates:

$$\begin{aligned} n'(X',0,Z')/n_0 == 1-(\frac{\beta_0}{\pi})^{3/2}\int_0^{2\pi}d\varepsilon\int_0^{\theta_0}\sin\phi d\phi[\frac{U_0a}{2\beta_0}\exp(-\beta_0U_0^2a^2)+ \\ \frac{1}{2}(U_0^2a^2+\frac{1}{2\beta_0})\sqrt{\frac{\pi}{\beta_0}}[1+sign(U_0a)erf(U_0\mid a\mid\sqrt{\beta_0})]]\exp(-\beta_0U_0^2(1-a^2))+ \\ \frac{1}{4\pi n_0}\int_0^{2\pi}d\varepsilon\int_0^{\theta_0}n_w\sin\phi d\phi \end{aligned} \tag{12}$$

where $a = \sin\phi\cos\varepsilon\cos(\pi/2-\alpha)+\cos\phi\sin(\pi/2-\alpha)$; and with $K = \sin^2\theta\cos\varepsilon$ and $b = -U_0a$:

$$\begin{aligned} \sqrt{\beta_0}U'(X',0,Z') = \frac{n_0U_0\sin\alpha}{n\sqrt{2RT_0}}-(\frac{\beta_0}{\pi})^{3/2}\frac{n_0}{n}\int_0^{2\pi}d\varepsilon\int_0^{\theta_0}[K(\frac{b^2}{2\beta_0}+\frac{1}{2\beta_0^2})-\frac{3b^2K}{2\beta_0}\exp(-\beta_0b^2)+ \\ (-\frac{3bK}{2\beta_0}-b^3K)\sqrt{\frac{\pi}{\beta_0}}[1+sign(U_0a)erf(U_0\mid a\mid\sqrt{\beta_0})]+\frac{3b^2K}{2\beta_0}\exp(-\beta_0b^2)] \\ \exp[-\beta_0U_0^2(1-a^2)]d\theta+\frac{1}{2\pi n\sqrt{\pi}}\sqrt{\frac{T_w}{T_0}}\int_0^{\theta_0}\sin^2\phi\cos\phi d\phi\int_0^{2\pi}n_w(\theta',\varepsilon)d\varepsilon, \end{aligned} \tag{13}$$

Similary we can obtain W(X', 0, Z'). The temperature field is:

$$\begin{aligned} \frac{T}{T_0} = \frac{T_w}{4\pi nT_0}\int_0^{2\pi}d\varepsilon\int_0^{\theta_0}\sin\theta' n_w d\theta'+\frac{n_0}{n}(1+\frac{U_0^2}{3RT_0})-\frac{1}{3nRT_0}\int_0^{2\pi}d\varepsilon\int_0^{\theta_0}\sin\theta' n_w(\frac{\beta_0}{\pi})^{3/2}\exp[-\beta_0U_0^2(1-a^2)] \\ ((-\frac{5b}{4\beta_0^2}-\frac{b^3}{2\beta_0})\exp(-\beta_0b^2)+(\frac{3}{4\beta^2}+b^4+\frac{3b^2}{\beta_0})[1-sign(b)erf(\mid b\mid\sqrt{\beta_0})])d\theta'-\frac{U^2+W^2}{3RT_0} \end{aligned} \tag{14}$$

We performed one DSMC simulation and compared the results with analytical results. Figures 4 and 5 show the contours of normalized number density, U-velocity components and temperature for the sphere case. In general, the analytical and numerical results are essentially identical. It is also noticeable that at the same location as the cylinder case[9], the number density value for sphere is smaller. This is because gas is much easier to flow around a sphere while a cylinder is more effective to block gas molecules.

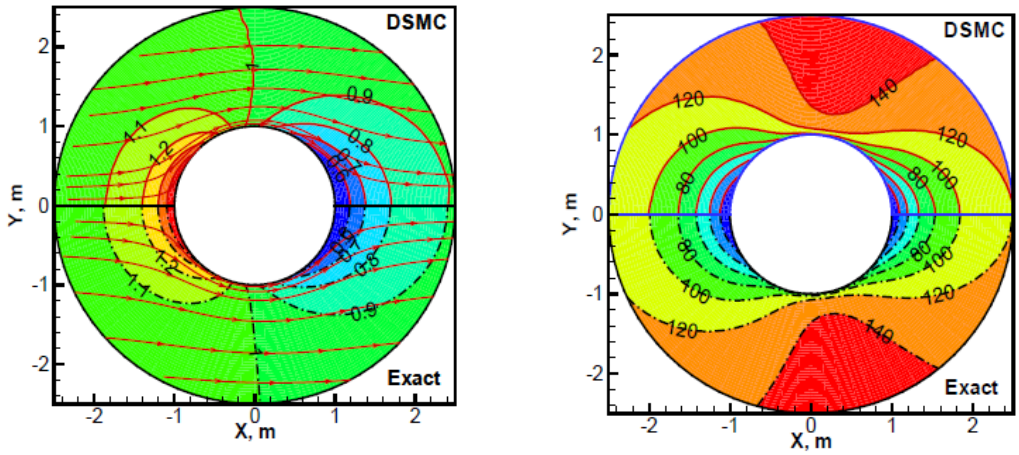

FIGURE 4. Normalized density contours and streamline (left), and U-velocity contours (right), for collisionless gas flows around a sphere. S=0.5, T_0=200 K, T_w=300K.

It is also meaningful to compare some past results of centerline density distribution in the literature, because of its important applications in space engineering. For the back and ram sides of a spherical spacecraft, there are some simple formulae [10] for the center line density distributions: for cases with hyper-velocity free stream, and reflections on the spherical object are completely reflective. However, for locations close to the sphere, the past results are not accurate. Figure 5 (right) shows a comparison with larger discrepancy; the equation in [10] provides negative density value at the back stagnation point. Even though the equation in [10] provides a very concise format, we need to keep in mind that it is an approximation only valid at locations far from the object. For the ram side, in general, at different locations along the centerline, the density is a function of the free stream mean velocity U_0 but the equation in [10] does not include any factor of free-stream velocity. Also, the past equation predicts that on the front stagnation point of the sphere, the normalized density ratio is a fixed value of 2.0 regardless of free stream velocity. This is not accurate because of two reasons which are clearly shown by Eqn.(11). First, if the free stream mean velocity is not large enough, then only a fraction of, rather than all of, the free stream particles can reach the front stagnation point. Secondly, for completely diffuse wall reflections, the temperature ratio T_w/T_0 is a key factor in determining n_w. These two factors result in different normalized number density values at the stagnation point. The density formula from this study can lead to more accurate centerline density distributions[9], no matter the location is far from or close to the object.

CONCLUSIONS

We have reported our progress on collisionless gas flows over a plate or a spherical object. By integrating the VDFs with different moments, we obtained complex but accurate solutions for density, velocity components, and temperature. The DSMC simulations yield almost identical results, indicating the approaches and results for this study are valid. The sphere case yield very satisfactory agreement as well.

We want to emphasize several significant points here to conclude this paper: 1) these solutions are applicable to to many problems described in the introduction part; 2) The evaluation of these exact solutions, requires less than one minute for each case; by comparison, the DSMC simulations require several days; 3) it seems there is no previous exact analytical solution for the same problems in the literature, even though there are numerical results in textbooks. The past numerical results cannot explicitly illustrate the effects of different physical and geometrical factors. By comparison, the exact solutions from this study overcome those defects. The exact solutions from this study complement those exact solutions in the literature about surface properties. 4) These exact solutions can serve as benchmark cases for simulation methodology development, or serve as base solutions to study less rarefied flow situations, for example, with a linearized Boltzmann equation method.

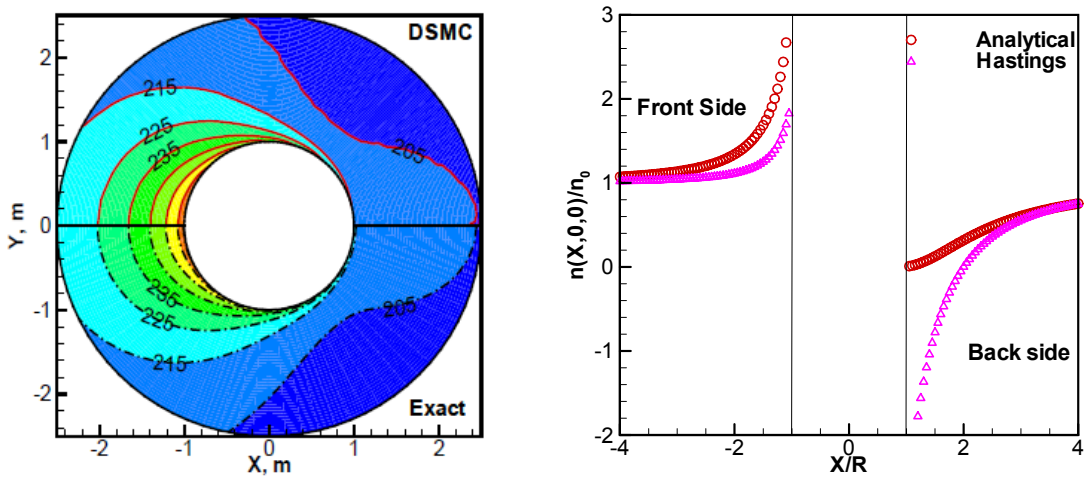

FIGURE 5. Collisionless gas flows around a sphere. Left: temperature contours, S=0.5, T_0=200 K, T_w=300K; Right: density distributions along the front and back sides of the centerline. S=2.0, T_0=200 K, T_w=300K.

REFERENCES

1. P.S., Epstein, P. S., *Zeitschrift fuer Physik*, Vol. 54, 537–563,1929.
2. C.Y., Liu, "Kinetic Description of Conductive Heat Transfer From a Fine Wire", Ph.D. Thesis, Caltech, 1962.
3. G.A., Bird, *Molecular Gas Dynamics and the Direct Simulation of Gas Flows*, Claredon Press, 1994.
4. L., Loth, *AIAA Journal*, Vol.46, No.9, pp.2119-2228.
5. J. A. Storch ,"Aerodynamic Disturbance on Spacecraft in Free-Molecular Flow",Aerospace Report 2003(3397)-1
6. C. Cai, and I.D., Boyd, *J. Spacecraft and Rockets,* Vol.44, No.2, pp.619-624, 2007.
7. R. Narasimha, *J. Fluid Mechanics*, Vol. 10, pp.371, 1961.
8. C. Cai, and K.R., Khasawneh, *J. Vacuum Science and Technology (A)*, 27(4), 2009.
9. C. Cai, K. Khasawneh, and M. Wei, *J. Spacecraft and Rocket*, 46(6), 2009.
10. D. Hastings and H. Garrett, *Spacecraft-Environment Interactions,* Cambridge University Press, New York, 1996.